Electronic Supplementary Material (ESI) for Journal of Materials Chemistry C.

Supporting Information

Effective encapsulation method for highly stable perovskite solar cells by introducing UV absorber with biomimetic textures and heat sinker with reduced graphene oxide composite layer

Fuqiang Li [a], Chaoqun Ma [b], Xiaofeng Huang [c], Yoomi Ahn [a], Danbi Kim [a], Eunhye Yang [a], Junpeng Xue [a], Bo Ram Lee [a], Junghwan Kim [d], Yongchao Ma [e] and Sung Heum Park *[a]

* Corresponding authors.

E-mail addresses: spark@pknu.ac.kr (S.H.Park)

1. Materials and methods

Materials: All chemicals were purchased from Sigma-Aldrich (Australia), Alfa Aesar (Australia), and Great Cell Solar (Australia) and used without further purification. Fluorine-doped tin oxide on glass (FTO glass, 7 Ω sq^{-1}) was purchased from Great Cell Solar. Norland Optical Adhesive (NOA, NOA-63) was purchased from KÖMMERLIN (Germany). The rGO nanosheet was synthesized by a modified Hummers' method, as previously reported.[1] To develop the rGO/NOA-63 composite layer, rGO was added into NOA-63 solution (NOA-63: rGO weight ratio 99: 1) and dispersed by sonication for 30 min. The reaction mixture was stirred at 25 °C for 2 h.

Materials Synthesis: Formamidinium lead triiodide ($FAPbI_3$) powder was synthesized by retrograde method.[2] In detail, PbI_2 and FAI (1:1 molar ratio) were dissolved in 2ME (0.8 M) first and then filtered using a polyvinylidene fluoride filter with 0.45 μm pore size. The filtered solution was placed in a flask incubated in an oil bath at 120 °C for 1 h under continuous stirring. The resulting black powder was filtered using a glass filter and dried at 60 °C for 72 h.

Solar cell fabrication: FTO glass was cleaned with Hellmanex solution (Sigma-Aldrich, Australia), acetone, isopropanol and UV-ozone.

A ~20 nm thick dense blocking layer of TiO_2 was deposited by spray pyrolysis of a solution of titanium diisopropoxide bis(acetylacetonate) in isopropanol (mass fraction = 8.4%) at 450 °C.

For the fabrication of the mesoporous TiO_2 layer (m-TiO_2), a suspension containing 150

mg/mL Dyesol 30 NR-D TiO_2 paste (GreatCell Solar, Australia) dispersed in ethanol was spin-coated at 4000 rpm (acceleration of 2000 rpm/s) for 15 s on top of the c-TiO_2 layer. The substrates were then annealed at 100 °C for 10 min followed by sintering at 500 °C for 30 min.

The perovskite precursor solution was prepared by dissolving 1550 mg $FAPbI_3$ and 61 mg MACl with 1 mL DMF/DMSO (4:1). The perovskite solution was filtered with a PVDF filter (0.2 μm) and then 70 μL of the filtered perovskite solution was spread onto different ETLs at 8000 rpm for 50 s. During the spin-coating, 1 mL diethyl ether was dropped on the perovskite film at 10 seconds. The resulting film was annealed at 150 °C for 15 mins and 100 °C for 30 mins on a hotplate. After the substrates cooling down, octylammonium iodide/IPA solution (15 mM) was spin-coated on the perovskite layer at 3000 rpm for 30 s.

For the hole transport layer, the Spiro-OMeTAD solution was spin-coated on the perovskite layer at 4000 rpm for 30 s. Spiro-OMeTAD (90 mg/mL in CB) was doped with 39 μL 4-tert-butylpyridine (tBP), 23 μL Li-bis(trifluoromethanesulfonyl)imide (Li-TFSI) (520 mg/mL in acetonitrile) and 5 μL FK209 (180 mg/mL in acetonitrile).

The Au electrode was deposited onto the Spiro-OMeTAD layer using a thermal evaporation system. 100 nm thick Au was deposited at 2 Å/s under a pressure of 10^{-6} Torr.

Replication of the plants' epidermal surface onto a UV absorption layer: First, the fresh petal was fixed in a polydimethylsiloxane (PDMS) mold. The PDMS was hardened at 60 °C on a hot plate for 4 h and then separated from the petal, which left a flexible petal

PDMS stamp. Plant remnants on the PDMS were removed in an ultrasonic bath with isopropanol.

In order to replicate the structures into UV-absorbing layer, the following steps were carried out: a drop (around 50 μL) of UV-curing adhesive UV-9/NOA-63 was placed on the glass substrate and the PDMS mold was carefully pressed into the drop, ensuring that any air bubbles were directed to the sample edges. After 1 min of UV exposure (at 1.5 mW cm^{-2} UV radiation power), the PDMS stamp was separated from the cured NOA-63 to be reused for further replicas (**Figure S2**).

PeSC packaging: To ensure good hermetic packaging by blanket encapsulation, clean and residue free edges around the active PeSC area were prepared. The UV-curable glue (rGO/NOA-63) was deposited on the active area and a 1–2 mm thick cover glass was laid on top. The glue was cured by gently pressing over the cover glass and applying about 30 s of UV irradiation.

Characterization of the UV absorption layer: Differential scanning calorimetry (DSC) was employed to evaluate the glass transition temperature (T_g) of the NOA-63 material, by means of a Mettler-Toledo DSC/823e instrument at a scan rate of 20 °C min^{-1} under N_2 flux. Values of T_g were obtained from the second heating ramp. The thermal stability of the UV-coating was evaluated by means of thermo-gravimetric analysis (TGA) on fully crosslinked solid state samples with a Q500 TGA system (TA Instruments) operated from ambient temperature to 800 °C at a scan rate of 10 °C min^{-1} both in air and under flowing N_2. The surface morphologies of the patterned NOA films were inspected using a field-

emission scanning electron microscope (FESEM, JEM-2100 F, JEOL LTD). The water contact angle was measured using dynamic contact angle equipment (DCA, Phoenix 300, SEO).

PeSC characterization: The solar cells were measured using a solar simulator (Newport-Oriel 94083A) together with a Keithley source meter 2400. Solar cells were covered with a black metal mask limiting the active area to 0.08 cm^2 and reducing the influence of the scattered light. The light intensity was calibrated to 100 mW/cm^2 using a Si-reference cell certified by NREL for the measurements. The conventional *J-V* curves were measured under both forward and reverse scans. The solar cell IPCE measurement system (Solar Cell Scan 100) is used to analyze the incident photon-electron conversion efficiency (IPCE).

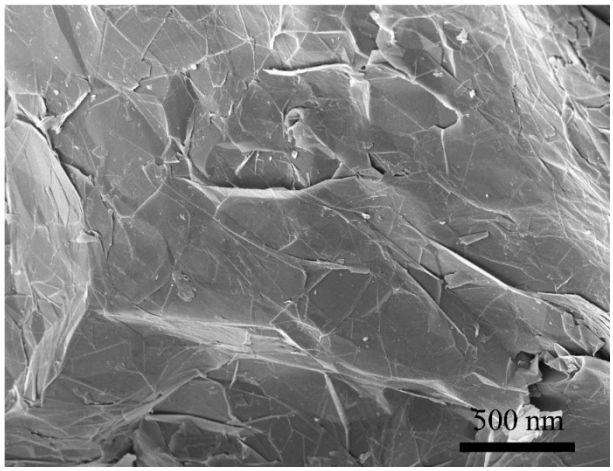

Figure S1. SEM image of synthesized reduce graphene oxide (rGO).

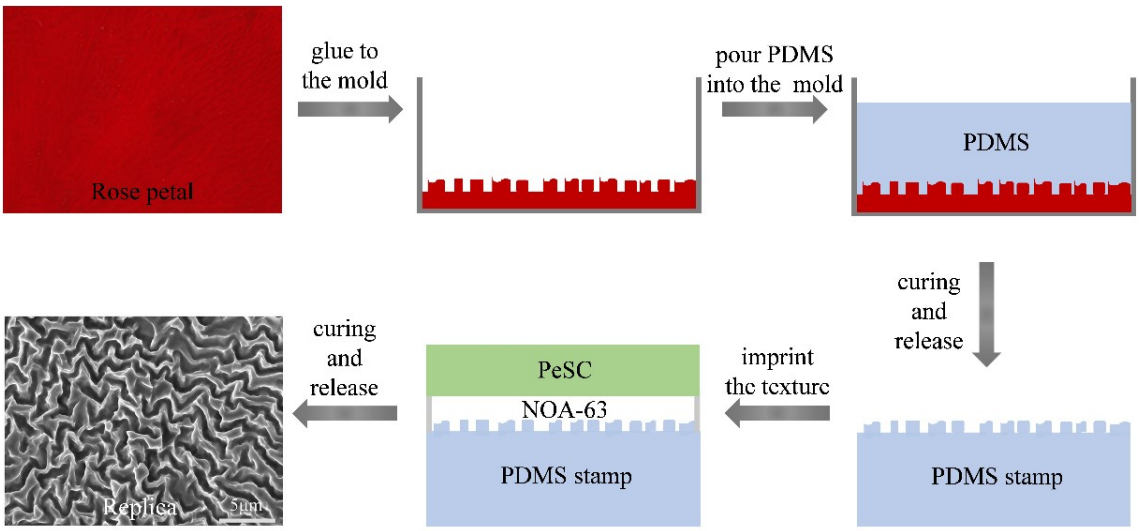

Figure S2. Schematic of the replication process.

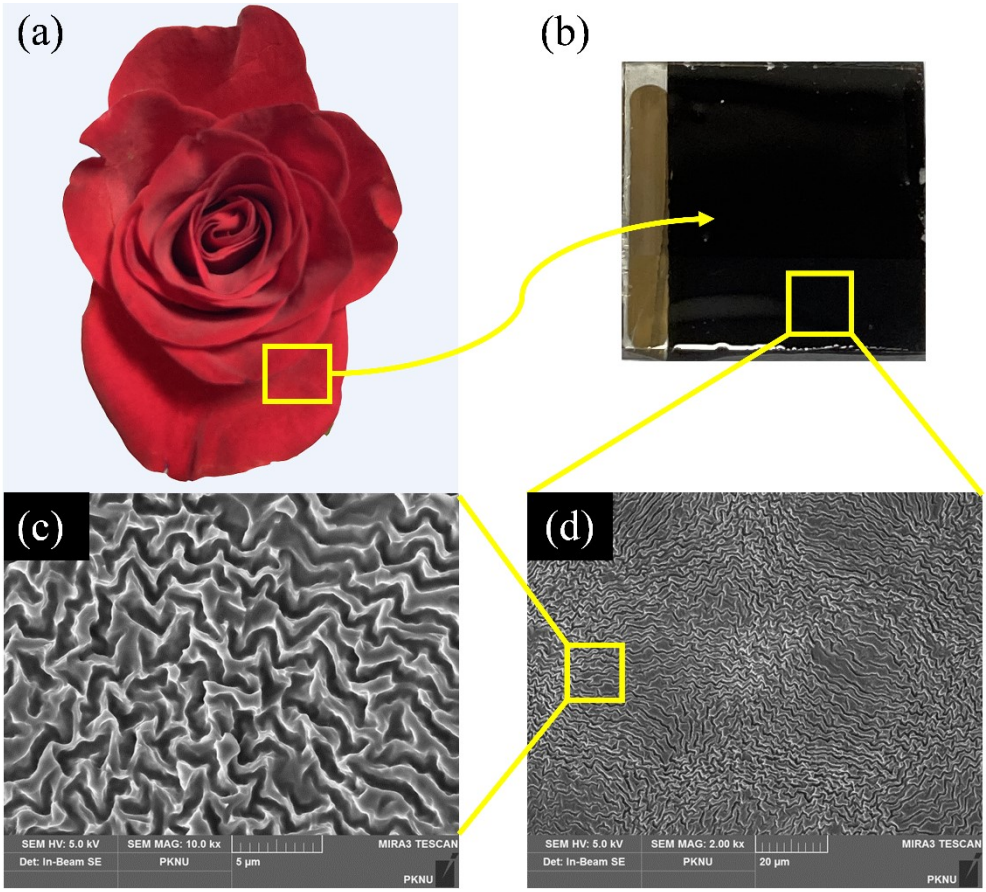

Figure S3. (a) Photograph of the original rose petals. (b) Photograph of the UV-absorbing layer with the replicated rose surface texture. (c, d) The SEM images of the replicated rose surface texture at different magnifications.

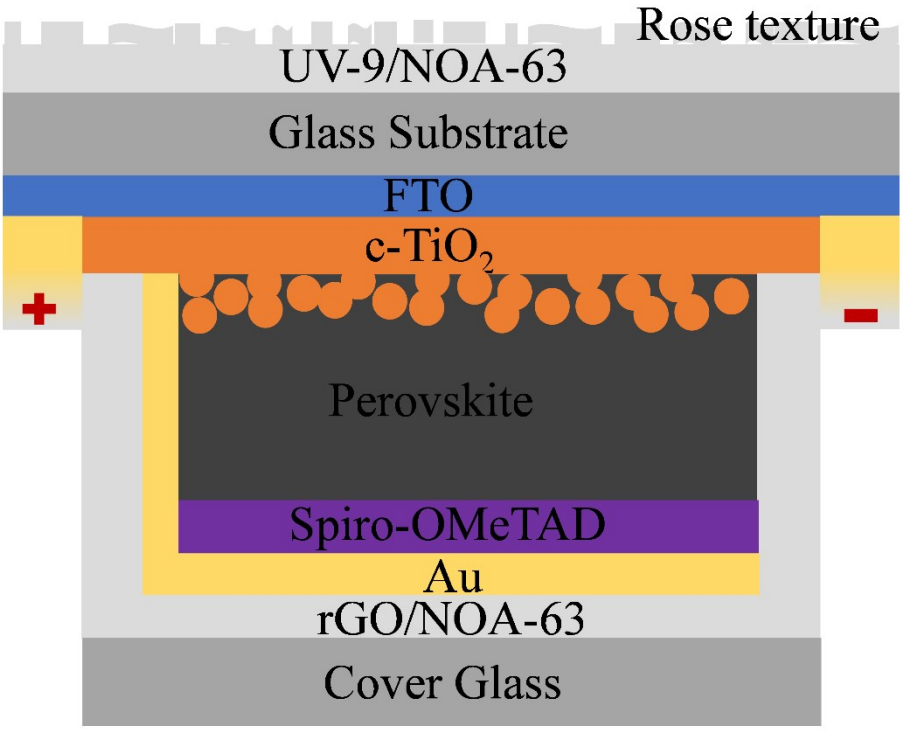

Figure S4. Structure of PeSC encapsulated with rGO/NOA-63 encapsulation film.

2. Optical properties of the UV-absorbing layer

To investigate the effect of the concentration of UV-9 hosted in the NOA-63 matrix on the optical properties of the UV-absorbing layer, absorption spectra of the UV-absorbing layer at increasing UV-9 concentrations were collected on 5 μm thick UV-absorbing layer, as shown in **Figure S5**. As expected, a progressive increase in UV-9 concentration leads to a correspondingly increased absorption intensity (absorbance).

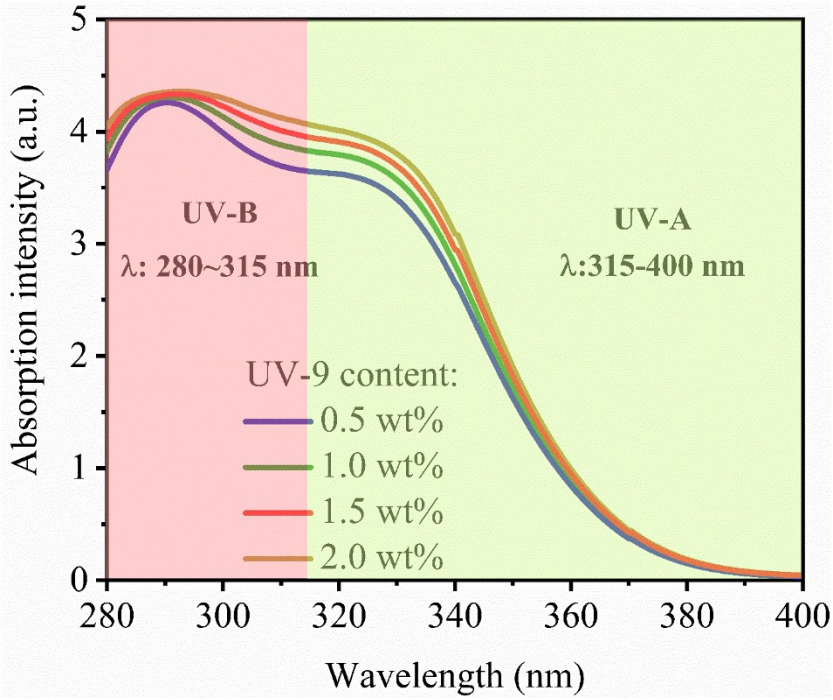

Figure S5. UV-vis absorption spectra of the UV-absorbing layer at increasing UV-9 concentration.

3. Thermal properties of the UV-absorbing layer

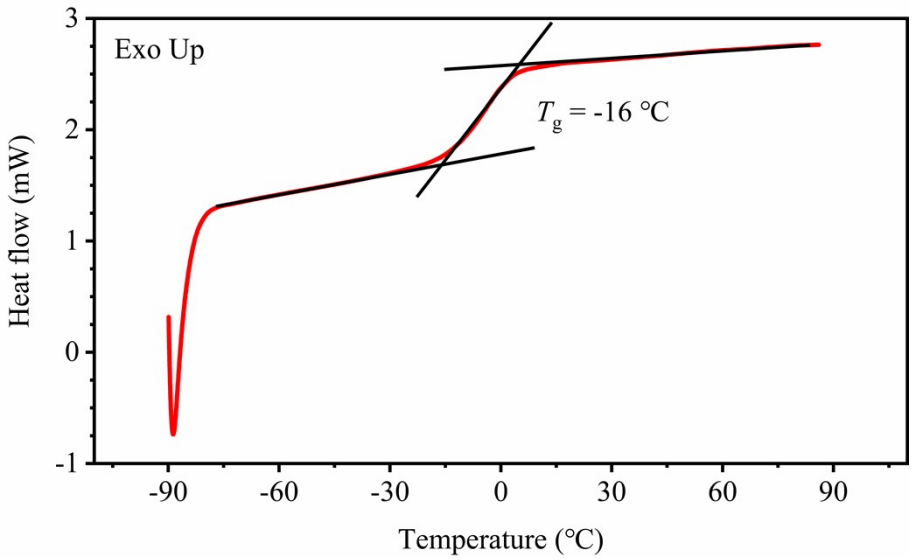

Figure S6. DSC trace of the UV-absorbing layer.

DSC thermogram of the UV-absorbing layer. As segmented block polyurethane, UV-absorbing layer is expected to possess two different glass transition temperatures (T_g) values. However, the curve exhibits only one T_g of –16 ℃. This may be due to the fact that the NOA-63 and UV-9 are well-dispersed and blended within the films; thus, oligomer consists of one phase. The DSC thermograms of the copolymer/absorbent blends showed only one T_g, which revealed the homogeneous system of absorbent/copolymer and the miscibility of the absorbent with the copolymer.

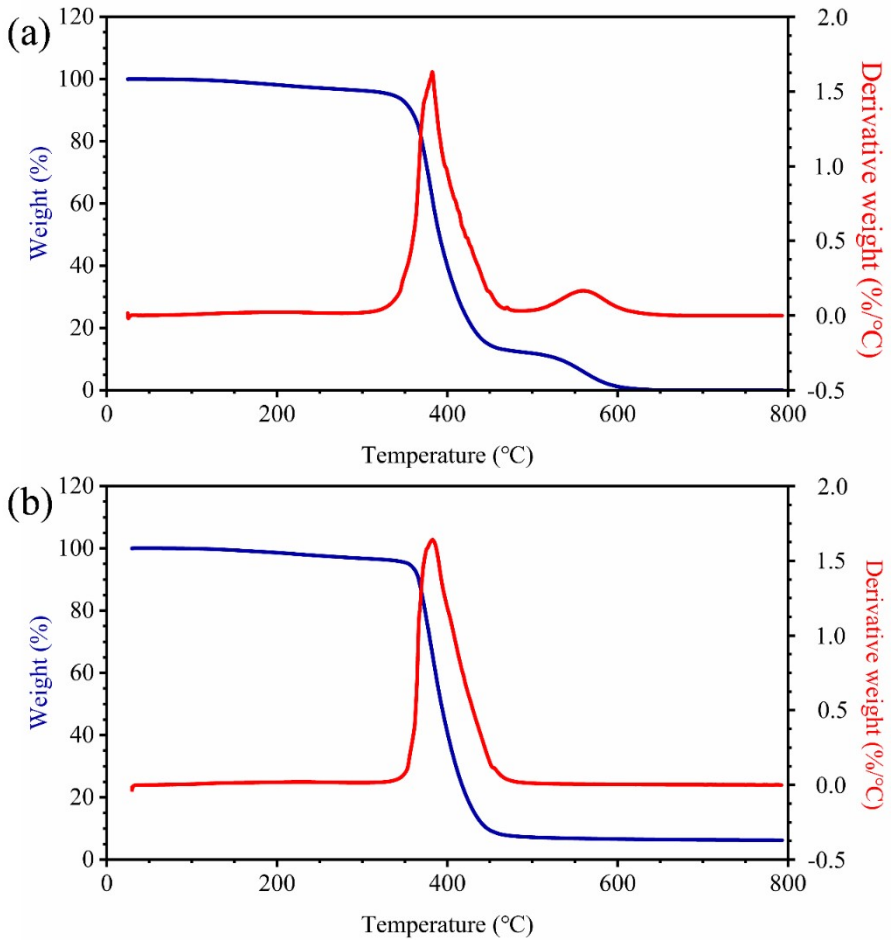

Figure S7. TGA thermograms of the UV-absorbing layer carried out (a) in air and (b) in nitrogen atmosphere.

4. Surface wettability behavior of the UV-RT

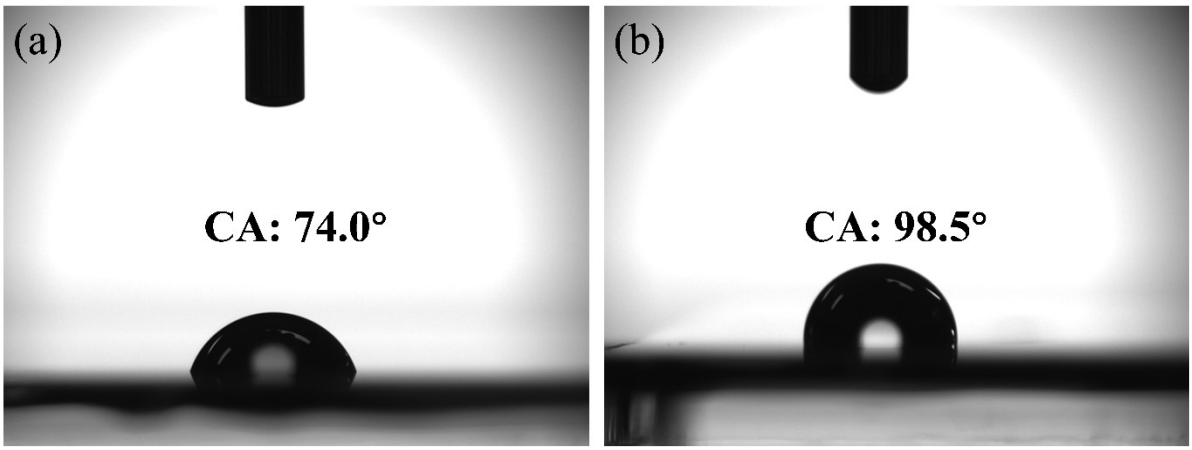

Figure S8. Images of water drops on surfaces of (a) UV-absorbing layer and (b) surface rose texture UV-absorbing layer.

Figure S8 shows surface images of liquid drops; rose texture on UV-absorbing layer increase the contact angle from 74.0° to 98.5°. The rose texture increases the surface roughness, thus increasing the contact angle. This means that the surface of the surface rose texture UV-absorbing layer is more hydrophobic. Micropatterning thus enables reduced water condensation and dust accumulation. Therefore, the UV-RT may facilitate self-cleaning ability.

5. Optical properties of the UV-RT

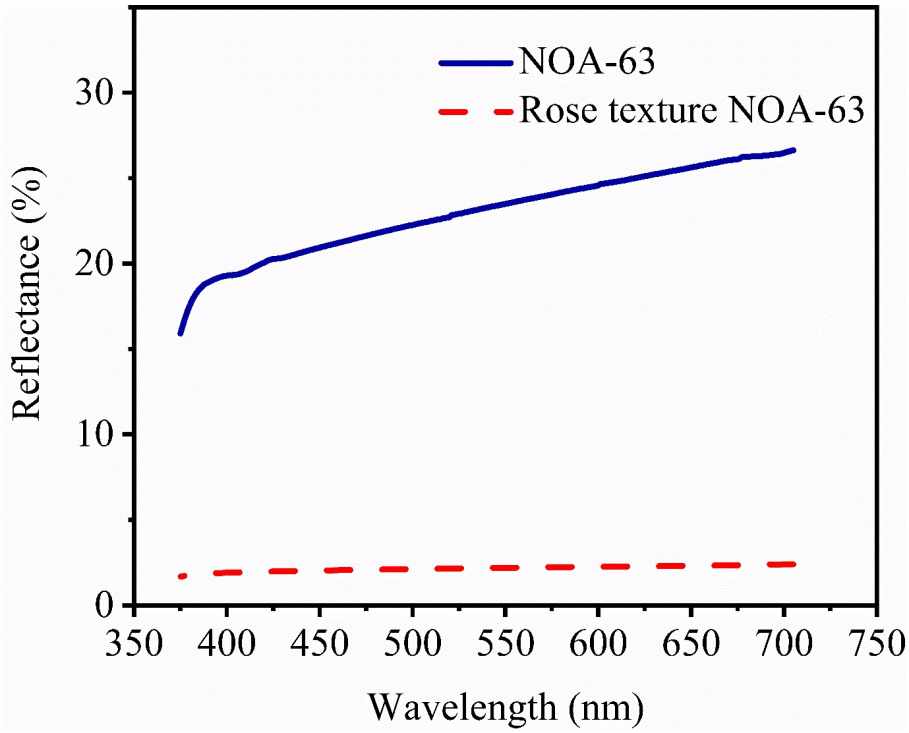

Figure S9. The reflectance spectra of NOA-63 and surface rose texture NOA-63.

The flat NOA-63 film shows the average reflectance of 22.98% in the visible wavelength range between 400 nm and 700 nm. However, the average reflectance of the rose texture NOA-63 film is 2.16%. This is attributed to the surface micro-/nano hierarchical structure effect, which decreases light reflection. In addition, the increased transmission of the rose texture NOA-63 film is attributed to the light scattering on the patterned surface.

6. The temperature of PeSCs with the encapsulation layer

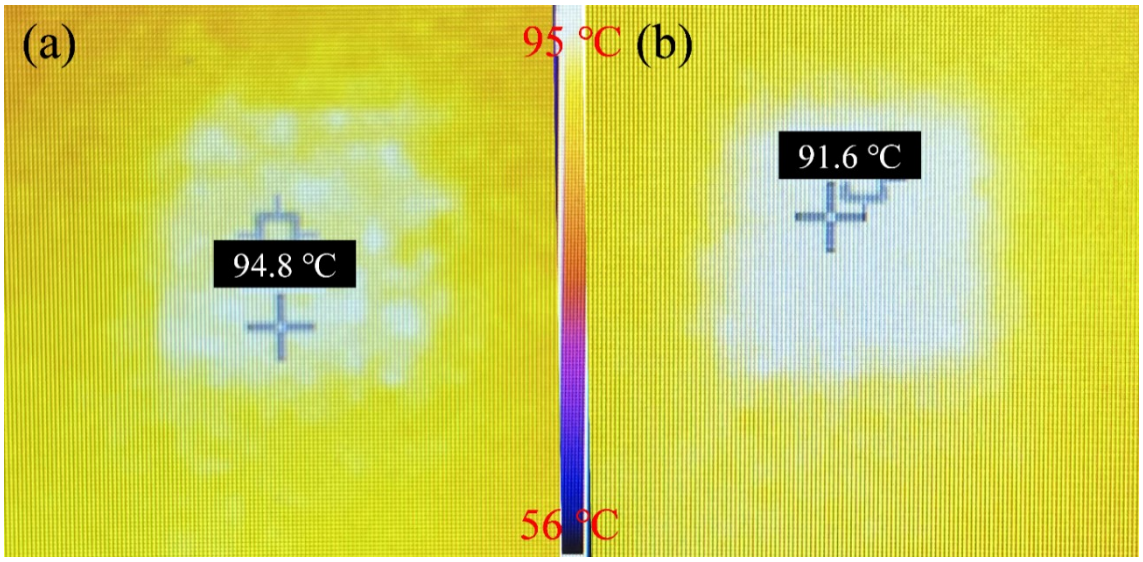

Figure S10. (a) The NOA-63 layer-coated glass plate (NOA-63/glass) and (b) the rGO/NOA-63 layer-coated glass plate (rGO/NOA-63/glass) were placed on the hot plate at 95 °C and heated from the bottom of the glass plate.

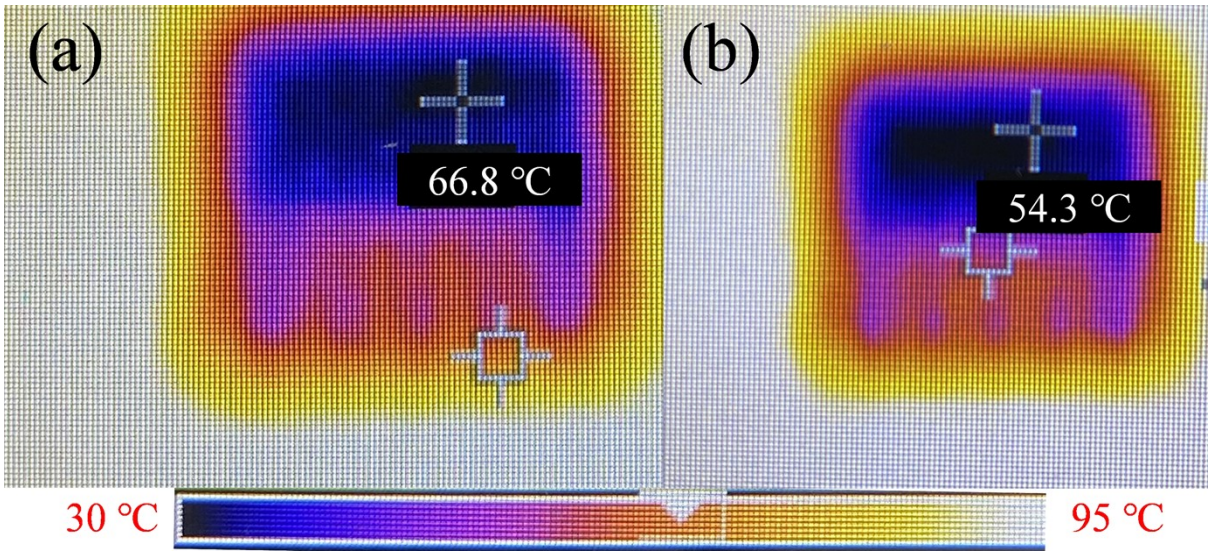

Figure S11. Infrared thermal camera images of (a) the NOA-63 coated PeSC and (b) the rGO/NOA-63 coated PeSC. (Hot plate at 95 °C)

7. UV stability of organic solar cells

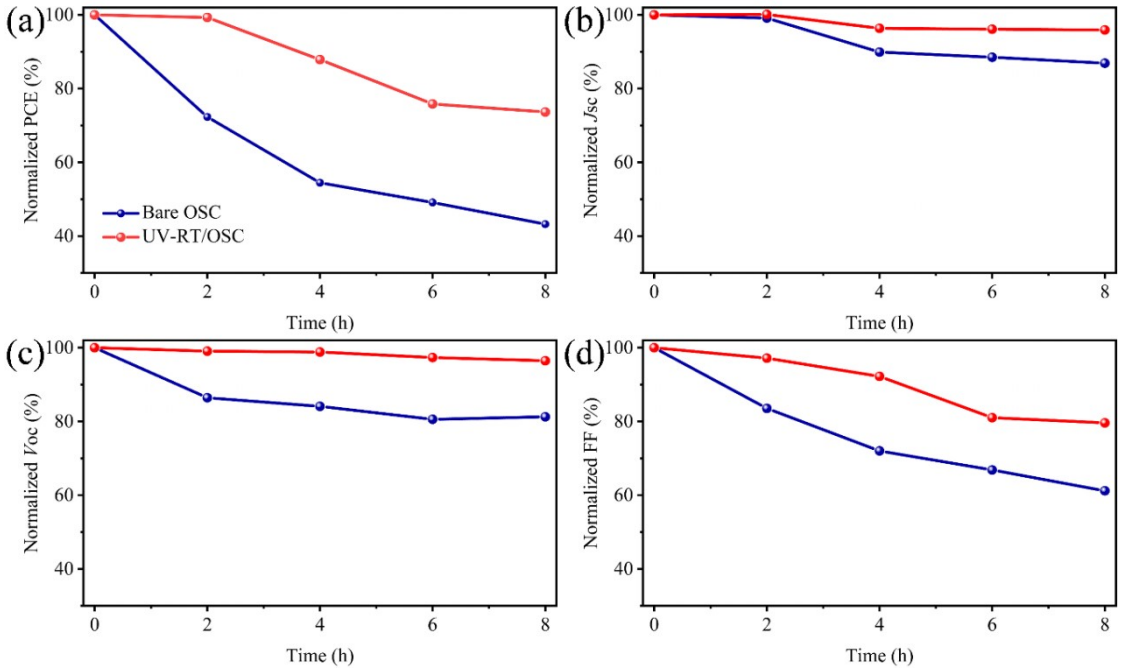

Figure S12. UV stability of OSCs under 60 mW/cm^2 UV light (wavelength of 365 nm) for 8 h in nitrogen condition.

Table S1. Photovoltaic parameters of PeSCs coated with the UV-AR loaded with different amounts (0.5 to 2 wt. %) of UV-9.

Average values for uncoated devices are also show for comparison purposes. Each experimental condition was reproduced 5 times on different devices; solar cells were tested under 1 Sun, AM1.5G, at a scan rate of 5 mV s^{-1} and with a mask are of 0.08 cm^2.

UV-9 (wt%)	*J*sc (mA/cm^2)	*V*oc (V)	FF (%)	PCE (%)
Control	24.35±0.37	1.08±0.02	80.14±1.41	21.08±0.63
0.5	25.50±0.43	1.08±0.02	79.25±1.53	21.83±0.80
1.0	25.55±0.28	1.09±0.01	79.92±1.64	22.26±0.45
1.5	24.87±0.51	1.07±0.04	79.35±1.27	21.12±1.08
2.0	24.26±0.59	1.09±0.03	79.25±1.78	20.97±1.31

References

1. A. Hassani, P. Eghbali, F. Mahdipour, S. Wacławek, K.-Y. A. Lin and F. Ghanbari, *Chemical Engineering Journal*, 2023, **453**, 139556.
2. M. Kim, J. Jeong, H. Lu, T. K. Lee, F. T. Eickemeyer, Y. Liu, I. W. Choi, S. J. Choi, Y. Jo, H.-B. Kim, S.-I. Mo, Y.-K. Kim, H. Lee, N. G. An, S. Cho, W. R. Tress, S. M. Zakeeruddin, A. Hagfeldt, J. Y. Kim, M. Grätzel and D. S. Kim, *Science*, 2022, **375**, 302-306.